Robust European Call Option Pricing via Linear Regression

Ahmad W. Bitar

Detection of subpixel targets with low fill-fraction: An application to hyperspectral imagery

Ahmad W. Bitar
Laboratory of Computer Science and Digital Society
Université de Technologie de Troyes
Troyes, France
ahmad.bitar@utt.fr

***Abstract*—In hyperspectral imagery, each subpixel target is well known as the target of interest that occupies only a fraction of the pixel area. The remaining part of the pixel is then filled with the background (at the same spatial location). In this paper, we mainly discuss a hyperspectral target detector that is represented as a sparse hyperspectral image (HSI) that ideally contains only subpixel targets with the background suppressed. More precisely, with the help of a pre-learned target dictionary constructed from some online spectral libraries, the given HSI can be decomposed into a sum of low-rank background HSI and a sparse target HSI, where the latter can be directly used as the target detector. However, with this matrix separation model, the detection of the target of interest may fail (or not succeed without a lot of false alarms) when the subpixel target has a very low fill-fraction and especially when its spectra is well matched to the surroundings. To well alleviate this serious real challenge, we prove via some synthetic experiments that learning an additional background dictionary, and when included in the matrix separation model, would be crucial.**

***Index Terms*—Hyperspectral target detection, sparse target HSI, background dictionary, target dictionary, low target fill-fraction.**

I. Introduction

The hyperspectral remote sensing system [1]–[8] has essentially four basic parts: (1) the illumination source (e.g., the Sun in passive remote sensing); (2) the atmospheric path; (3) the target scene; and (4) the airborne hyperspectral imaging sensor. In hyperspectral imagery, pixels are represented by vectors whose entries correspond to spectral bands, and images are represented by 3-D hypercubes. One of the most important applications of hyperspectral imagery is target detection [1], [2], [9]–[15], which can be viewed as a binary classification problem where pixels are labeled as target or background based on their spectral characteristics. Hyperspectral imagery has many applications in areas such as military [11], [16], [17], agricultural [18], [19], mineralogy [20], and medical fields. Its rich spectral information allows for a more accurate material identification. However, the greatest challenge lies in modeling the variation of data due to material spectral variability, atmospheric conditions, and sensor noise.

The hyperspectral image (HSI) contains both pure and mixed pixels [2], [3]. A pure pixel represents only one single material which can be either a pure target or a pure background; whereas a mixed pixel represents an aggregation of multiple materials where the result can be either a pure target, a pure background, or a mixture between the target and background in the corresponding spatial location. It is well known that in hyperspectral imagery, every test pixel is represented by a replacement signal model [2]. That is,

$$\mathbf{x} = \alpha\,\mathbf{t} + (1-\alpha)\,\mathbf{b}\,,$$

where $\mathbf{x}$ is the hyperspectral test pixel, $\mathbf{t}$ is the spectrum of the target, $\mathbf{b}$ is the spectrum of the background located at the same spatial location of the target, and $\alpha \in [0,\,1]$ is the target fill-fraction. When $\alpha = 0$, $\mathbf{x}$ is a background pixel (that is, fully occupied by the background material); whereas when $\alpha \in (0,\,1]$, the pixel $\mathbf{x}$ is fully ($\alpha = 1$) or partially ($0 < \alpha < 1$) occupied by the target material.

A prior information about the target spectral signature is often provided to the user and can be collected from some online spectral libraries. Given this target information, a novel hyperspectral target detector has recently been developed in [21]–[23], mainly based on the assumption that the background is low-rank and the targets are spatially sparse. More precisely, with the great help of a target dictionary constructed from some online spectral libraries, the original HSI can be decomposed into a low-rank background HSI (ideally contains only the background without the targets) and a sparse target HSI (ideally contains only the targets with the background is suppressed). The latter can be used directly as the target detector [23]. This detector behaves well in high dimensions and is well known to be (1) distributionally free, (2) invariant to atmospheric variations; and (3) independent of the completely unknown covariance matrix that needs to be efficiently estimated under a non-Gaussian assumption [12], [24]–[27] and especially in high dimensions [28]–[30]. In [23], this sparse hyperspectral target detector has been further evaluated to prove its efficiency in detecting two kinds of targets (e.g., Buddingtonite and Kaolinite) incorporated separately in a pure Alunite Background HSI for different values of fill-fraction α. The Buddingtonite target is considered an easy target with respect to the Alunite background since it is easily recognized based on its unique $2.12\mu m$ absorption band; The Kaolinite target presents overlapping spectral characteristics with the Alunite mineral and therefore is considered a very challenging target to detect. However, it has been observed from experiments in [23] that the proposed sparse hyperspectral target

detector fails to detect both targets without a lot of false alarms when α is small enough (e.g. ≤ 0.1).

In this paper, our main objective is to add a simple update to the proposed target detector in [23] to make it capable of detecting targets of interest without or with very few false alarms, even when the value of α is quite small. More precisely, our update concerns supporting the proposed background and target matrix separation model in [21]–[23] with an additional pre-learned background dictionary (ideally containing only the background pixels without the targets) [31], [32]. Note that further considering a background dictionary [31] in the work in [23] has already been proposed in [32] with some additional constraints about the spatial smoothness of the background pixels and the sparsity of the targets. Our main contribution in this paper is just to prove that by constructing a "perfect"[1] background dictionary may be sufficient to detect targets of interest without or with very few false alarms even when the value of α is quite small and especially when the target is well matched to the surroundings. The perfect background dictionary constructed, which helps us achieve the best target detection results, will be used as a reference for our subsequent research to compare with any other adaptive background dictionary construction approaches that we are currently working on.

This paper is structured along the following lines. First comes in section II a mathematical derivation of the sparse hyperspectral target detector already developed in [21]–[23] with our added simple update by incorporating an additional pre-learned background dictionary into the background and target matrix separation model. Section III presents synthetic experiments to gauge the effectiveness of our updated target detector for hyperspectral target detection. The paper ends with a summary and some directions for future work.

Summary of Main Notations: Throughout this paper, we depict vectors in lowercase boldface letters and matrices in uppercase boldface letters. The notation $(.)^T$ and $Tr\,(.)$ represent the transpose and trace of a matrix, respectively. A variety of norms on the matrices will be used. For example, $\mathbf{M}$ is a matrix, $M_{i,j}$ and $[\mathbf{M}]_{:,j}$ are the $(i,\,j)\,th$ element and jth column, respectively. The matrix $l_{2,1}$-norm is defined as $\|\mathbf{M}\|_{2,1} = \sum_j \left\|[\mathbf{M}]_{:,j}\right\|_2$. The Frobenius norm and the nuclear norm are defined as $\|\mathbf{M}\|_F = \left(\sum_i \sum_j M_{i,\,j}^2\right)^{\frac{1}{2}}$, and $\|\mathbf{M}\|_* = Tr\left(\mathbf{M}^T\mathbf{M}\right)^{\frac{1}{2}}$, respectively.

II. Our updated sparse hyperspectral target detector

In this section, our aim is to simply add a little update to the background and target matrix separation model proposed in [21]–[23]. More precisely, in addition to the prior target information, our update concerns adding a further prior information about the background.

[1]By "perfect" we mean that the background dictionary is purely constructed from the background pixels (without any target contamination) that completely represent all the background information of the given HSI.

Mathematical derivation of the sparse hyperspectral target detector in [21]–[23] with some additional little updates:

Consider that any given HSI is of size $h \times w \times p$, where h, w and p represent height, width, and total number of spectral bands, respectively. The sparse hyperspectral target detector is mainly derived in the following steps:

1) Let assume that the HSI contains only $0 < q << e$ target pixels, $e = h \times w$, each of the form:
$$\mathbf{x}_i = \alpha_i\,\mathbf{t}_i + (1-\alpha_i)\,\mathbf{b}_i\,, \quad i \in [1,\,q]\,,$$
where $\mathbf{t}_i \in \mathbb{R}^p$ represents the target of interest that replaces a fraction $\alpha_i \in (0,\,1]$ from the background $\mathbf{b}_i \in \mathbb{R}^p$ at the same spatial location.
2) Every $\{\mathbf{t}_i\}_{i\in[1,\,q]}$ consists of similar target materials[2], and thus, each can be represented as a linear combination of $N_t \geq 1$ common target samples $\left\{\mathbf{a}_j^t\right\}_{j\in[1,\,N_t]}$, where $\mathbf{a}_j^t = [a_{j,\,1}^t,\,a_{j,\,2}^t,\,\cdots,\,a_{j,\,p}^t]^T \in \mathbb{R}^p$ (the superscript t is for target), but weighted with different set of coefficients $\{\beta_{i,\,j}\}_{j\in[1,\,N_t]}$.
3) Every $\{\mathbf{b}_i\}_{i\in[1,\,q]}$ consists of similar background materials[3], and thus, each can be represented as a linear combination of $N_b \geq 1$ common background samples $\left\{\mathbf{a}_k^b\right\}_{k\in[1,\,N_b]}$, where $\mathbf{a}_k^b = [a_{k,\,1}^b,\,a_{k,\,2}^b,\,\cdots,\,a_{k,\,p}^b]^T \in \mathbb{R}^p$ (the superscript b is for background), but weighted with different set of coefficients $\{\theta_{i,\,k}\}_{k\in[1,\,N_b]}$.
4) Each of the q target pixels, $\mathbf{x}_i$, $i \in [1,\,q]$, can thus be represented as:
$$\mathbf{x}_i = \alpha_i \sum_{j=1}^{N_t}\left(\beta_{i,\,j}\,\mathbf{a}_j^t\right) + (1-\alpha_i)\sum_{k=1}^{N_b}\left(\theta_{i,\,k}\,\mathbf{a}_k^b\right)\,.$$
5) By rearranging the HSI into a two-dimensional matrix $\mathbf{D} \in \mathbb{R}^{e\times p}$, $e = h\times w$, the latter can be decomposed into a low-rank matrix ideally representing the pure background residing in the background subspace, a sparse matrix capturing only the targets of interest residing in the target subspace, and a noise matrix. More precisely, our updated background and target matrix separation model is:
$$\mathbf{D} = (\mathbf{A}_b\,\mathbf{L}_0)^T + (\mathbf{A}_t\,\mathbf{C}_0)^T + N_0\,, \tag{1}$$
where
- A_b is the background dictionary represented as $\begin{bmatrix} | & | & \cdots & | \\ \mathbf{a}_1^b & \mathbf{a}_2^b & \cdots & \mathbf{a}_{N_b}^b \\ | & | & \cdots & | \end{bmatrix} \in \mathbb{R}^{p\times N_b}$;
- A_t is the target dictionary represented as $\begin{bmatrix} | & | & \cdots & | \\ \mathbf{a}_1^t & \mathbf{a}_2^t & \cdots & \mathbf{a}_{N_t}^t \\ | & | & \cdots & | \end{bmatrix} \in \mathbb{R}^{p\times N_t}$;
- $\mathbf{L}_0 \in \mathbb{R}^{N_b\times e}$ is the low-rank coefficient matrix representation of D with respect to $\mathbf{A}_b$,

[2]It would be more realistic to assume that all $\{\mathbf{t}_i\}_{i\in[1,\,q]}$ consist of different target materials. However, it is not really necessary as one will end up with the same background and target separation matrix model in (1).

[3]It would be more realistic to assume that all $\{\mathbf{b}_i\}_{i\in[1,\,q]}$ consist of different background materials. However, it is not really necessary as one will end up with the same background and target separation matrix model in (1). What really matters is how the background dictionary $\mathbf{A}_b$ is constructed to efficiently represent all the background details of the given HSI.

ideally containing q columns each representing $(1-\alpha_i)[\theta_{i,1}, \cdots, \theta_{i,N_b}]^T$, $i \in [1, q]$;

- $(\mathbf{A}_b\, \mathbf{L}_0)^T \in \mathbb{R}^{e\times p}$ is the background HSI, ideally with $(e-q)$ rows representing the background pixels when $\alpha = 0$, and the remaining q rows represent the background pixels of the form $(1-\alpha_i)\left\{\mathbf{b}_i^T\right\}_{i\in[1,\,q]}$ (that is, after the $\alpha_i \mathbf{t}_i$ has been separated);
- $\mathbf{C}_0 \in \mathbb{R}^{N_t\times e}$ is a coefficient matrix that should be a sparse column matrix, ideally containing q non-zero columns each representing $\alpha_i[\beta_{i,1}, \cdots, \beta_{i,N_t}]^T$, $i \in [1, q]$;
- $(\mathbf{A}_t\, \mathbf{C}_0)^T \in \mathbb{R}^{e\times p}$ is the sparse target matrix, ideally with q non-zero rows representing $\alpha_i \left\{\mathbf{t}_i^T\right\}_{i\in[1,\,q]}$.

6) Recovering both $\mathbf{L}_0$ and $\mathbf{C}_0$ can be done iteratively via an alternating minimization optimization problems:
   - Update $\mathbf{L}^{(k+1)}$ as:
$$\underset{\mathbf{L}}{argmin}\left\{\tau\,\|\mathbf{L}\|_* + \left\|\mathbf{A}_b\,\mathbf{L} - \left(\mathbf{D}^T - \mathbf{A}_t\,\mathbf{C}^{(k)}\right)\right\|_F^2\right\}, \quad (2)$$
   - Update $\mathbf{C}^{(k+1)}$ as:
$$\underset{\mathbf{C}}{argmin}\left\{\lambda\,\|\mathbf{C}\|_{2,1} + \left\|\mathbf{A}_t\,\mathbf{C} - \left(\mathbf{D}^T - \mathbf{A}_b\,\mathbf{L}^{(k+1)}\right)\right\|_F^2\right\}, \quad (3)$$
   where $\tau > 0$ and $\lambda > 0$ are two parameters to be tuned manually and which control the rank of $\mathbf{L}$ and the sparsity level in $\mathbf{C}$, respectively. Both the matrix $\mathbf{L}$ and $\mathbf{C}$ can be estimated by various methods, among which we adopt the alternating direction method of multipliers (ADMM) as briefly outlined in Algorithm 1.
7) Once $\mathbf{L}$ and $\mathbf{C}$ are estimated, the matrix $(\mathbf{A}_t\,\mathbf{C})^T$ will be used directly for detection. More precisely, the target detector is just a sparse HSI, generated automatically from the original one, and which only contains the targets of interest with the background is suppressed.

III. Some synthetic experiments

We evaluate the updated hyperspectral target detector in section II for the detection of two different targets (Buddingtonite & Kaolinite) that are incorporated (with a very small target fill-fraction α) into an HSI of size $100\times 100\times 186$ that was manually created from 72 Alunite mineral background pixels (see the section of experiments and analysis in [23]). We follow the same experiments as in [23] to generate both the Buddingtonite and Kaolinite targets that will be incorporated into the Alunite HSI. For the selection of both τ and λ: we manually choose them to achieve the best target detection results without false alarms.

We construct the background dictionary A_b through the exact 72 Alunite minerals that were picked to construct the Alunite HSI in the experiment section in [23], that is, $N_b = 72$. Hence, we have $\mathbf{A}_b \in \mathbb{R}^{186\times 72}$. In this regard, the constructed $\mathbf{A}_b$ is a perfect dictionary, that is, it exactly represents the entire background details of the Alunite background HSI in [23]. Seven target blocks (each of size 6×3) are incorporated in the background Alunite HSI at a very small target fill-fraction α, and placed in long convoy formation. We are interested in three target detection scenarios:

Algorithm 1 Solving problem (2) and problem (3) via ADMM

Input: data matrix $\mathbf{D}$, $\mathbf{A}_t$, $\mathbf{A}_b$, parameter $\tau > 0$ and $\lambda > 0$.
Initialize: $k = 0$, $\mathbf{L}^{(0)} = \mathbf{0}$, $\mathbf{J}^{(0)} = \mathbf{0}$, $\mathbf{Z}_1^{(0)} = \mathbf{0}$, $\mathbf{C}^{(0)} = \mathbf{0}$, $\mathbf{F}^{(0)} = \mathbf{0}$, $\mathbf{Z}_2^{(0)} = \mathbf{0}$, $\rho_1^{(0)} = 10^{-4}$, $\rho_2^{(0)} = 10^{-4}$, $\max_{\rho_1} = 10^7$, $\max_{\rho_2} = 10^7$, $\epsilon = 10^{-4}$.
While not converged **do**:

1. Find solution to problem (2)**: while** not converged **do**:

1*a*) update $\mathbf{L}^{(k+1)}$ by:
$$\underset{\mathbf{L}}{argmin}\left\{\left\|\mathbf{A}_b\,\mathbf{L} - \left(\mathbf{D}^T - \mathbf{A}_t\,\mathbf{C}^{(k)}\right)\right\|_F^2 + \frac{\rho_1^{(k)}}{2}\left\|\mathbf{L} - \mathbf{J}^{(k)} + \frac{1}{\rho_1^{(k)}}\mathbf{Z}_1^{(k)}\right\|_F^2\right\}.$$

1*b*) update $\mathbf{J}^{(k+1)}$ by:
$$\underset{\mathbf{J}}{argmin}\left\{\frac{\rho_1^{(k)}}{2}\left\|\mathbf{J} - \left(\mathbf{L}^{(k+1)} + \frac{1}{\rho_1^{(k)}}\,\mathbf{Z}_1^{(k)}\right)\right\|_F^2 + \tau\,\|\mathbf{J}\|_*\right\}.$$

1*c*) update $\mathbf{Z}_1^{(k+1)}$ by:
$$\mathbf{Z}_1^{(k)} + \rho_1^{(k)}\left(\mathbf{L}^{(k+1)} - \mathbf{J}^{(k+1)}\right).$$

1*d*) update $\rho_1^{(k+1)}$ by:
$$min\left(1.1\,\rho_1^{(k)},\, \max_{\rho_1}\right).$$

1*e*) check the convergence condition:
$$\left\|\mathbf{L}^{(k+1)} - \mathbf{J}^{(k+1)}\right\|_F \le \epsilon.$$

2. Find solution to problem (3)**: while** not converged **do**:

2*a*) update $\mathbf{C}^{(k+1)}$ by:
$$\underset{\mathbf{C}}{argmin}\left\{\left\|\mathbf{A}_t\,\mathbf{C} - \left(\mathbf{D}^T - \mathbf{A}_b\,\mathbf{L}^{(k+1)}\right)\right\|_F^2 + \frac{\rho_2^{(k)}}{2}\left\|\mathbf{C} - \mathbf{F}^{(k)} + \frac{1}{\rho_2^{(k)}}\mathbf{Z}_2^{(k)}\right\|_F^2\right\}.$$

2*b*) update $\mathbf{F}^{(k+1)}$ by:
$$\underset{\mathbf{F}}{argmin}\left\{\frac{\rho_2^{(k)}}{2}\left\|\mathbf{F} - \left(\mathbf{C}^{(k+1)} + \frac{1}{\rho_2^{(k)}}\,\mathbf{Z}_2^{(k)}\right)\right\|_F^2 + \lambda\,\|\mathbf{F}\|_{2,1}\right\}.$$

2*c*) update $\mathbf{Z}_2^{(k+1)}$ by:
$$\mathbf{Z}_2^{(k)} + \rho_2^{(k)}\left(\mathbf{C}^{(k+1)} - \mathbf{F}^{(k+1)}\right).$$

2*d*) update $\rho_2^{(k+1)}$ by:
$$min\left(1.1\,\rho_2^{(k)},\, \max_{\rho_2}\right).$$

2*e*) check the convergence condition:
$$\left\|\mathbf{C}^{(k+1)} - \mathbf{F}^{(k+1)}\right\|_F \le \epsilon.$$

3. Stop when the convergence conditions are satisfied:
$$\frac{\left\|\left(\mathbf{A}_b\mathbf{L}^{(k+1)}\right)^T - \left(\mathbf{A}_b\mathbf{L}^{(k)}\right)^T\right\|_F}{\|\mathbf{D}\|_F} \le \epsilon,$$
$$\frac{\left\|\left(\mathbf{A}_t\mathbf{C}^{(k+1)}\right)^T - \left(\mathbf{A}_t\mathbf{C}^{(k)}\right)^T\right\|_F}{\|\mathbf{D}\|_F} \le \epsilon.$$

1) The seven target blocks correspond to only "Buddingtonite" targets. The target dictionary $\mathbf{A}_t$ is constructed in the same way as in the experiments in [23], that is, from three Buddingtonite target samples extracted from the online Advanced Spaceborne Thermal Emission and Reflection spectral library [33]. Hence, we have $\mathbf{A}_t \in \mathbb{R}^{186\times 3}$. Figure 1 exhibits the obtained target detection performance when the Buddingtonite target blocks are incorporated with $\alpha = 0.0002$. It is important to note that if we consider $\alpha < 0.0002$, the detection performance of our updated target detector will start to deteriorate and the false alarms will start to appear.

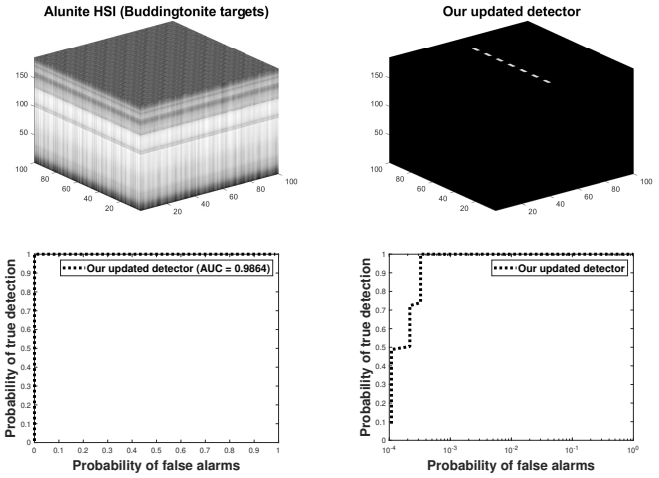

Fig. 1. From top left to bottom right: the original Alunite HSI containing the incorporated seven Buddingtonite targets with $\alpha = 0.0002$, our updated target detector, the ROC curve of our updated target detector, the ROC curve of our updated target detector for low probability of false alarms.

2) The seven target blocks correspond to only "Kaolinite" targets. The target dictionary $\mathbf{A}_t$ is constructed in the same way as in the experiments in [23], that is, from six Kaolinite target samples extracted from the online United States Geological Survey spectral library [34]. Hence, we have $\mathbf{A}_t \in \mathbb{R}^{186\times 6}$. Figure 2 exhibits the obtained target detection performance when the Kaolinite target blocks are incorporated with $\alpha = 0.002$. We choose this specific value of α because the updated detector will behave poorly in detecting the Kaolinite target pixels when $\alpha < 0.002$ and a lot of false alarms will appear.
3) The seven target blocks are distributed between four "Kaolinite" target blocks and three "Buddingtonite" target blocks. We are thus interested to detect two types of targets of interest (Buddingtonite and Kaolinite) in the same HSI. The target dictionary is constructed from the union of the Buddingtonite and Kaolinite target samples considered in the first two scenarios. Hence, we have $\mathbf{A}_t \in \mathbb{R}^{186\times 9}$. Figure 3 exhibits the obtained target detection results when the three Buddingtonite and four Kaolinite target blocks are incorporated with $\alpha = 0.0003$. When $\alpha < 0.0003$, the detection performance starts to deteriorate and a lot of false alarms start to appear.

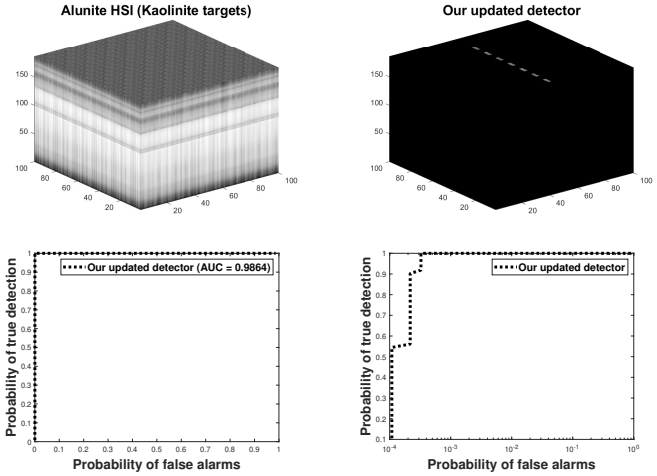

Fig. 2. From top left to bottom right: the original Alunite HSI containing the incorporated seven Kaolinite target blocks with $\alpha = 0.002$, our updated target detector, the ROC curve of our updated target detector, the ROC curve of our updated target detector for low probability of false alarms.

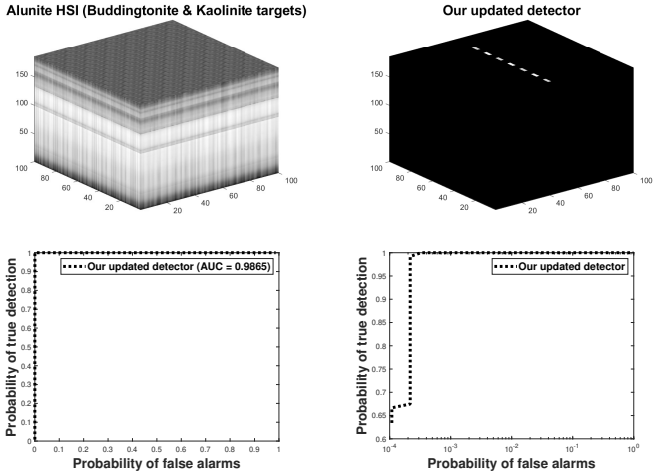

Fig. 3. From top left to bottom right: the original Alunite HSI containing four Kaolinite and three Buddingtonite target blocks with $\alpha = 0.0003$, our updated target detector, the ROC curve of our updated target detector, the ROC curve of our updated target detector for low probability of false alarms.

IV. Conclusion and Future Work

In this paper, we add a little update to the sparse and low-rank matrix decomposition model that has been developed in [21]–[23]. In addition to the prior target information (through a target dictionary $\mathbf{A}_t$), we have proved that further consideration of the prior background information (through a "perfect" dictionary $\mathbf{A}_b$) can significantly improve target detection, especially when the target fill-fraction α is very small and the target of interest is well matched to the surroundings. Regarding future enhancements, a likely first step would be to develop small-size adaptive background dictionary $\mathbf{A}_b$ construction approaches [35] which can generate a dictionary that is close to perfect. Other promising avenues for further research include improving the construction of the target dictionary [36]–[38] mainly due to the fact that there are usually not enough spectral signatures in the online spectral libraries.

REFERENCES

[1] G. Shaw and D. Manolakis, "Signal processing for hyperspectral image exploitation," *IEEE Signal Processing Magazine*, vol. 19, no. 1, pp. 12–16, Jan 2002.

[2] D. Manolakis, D. Marden, and G. Shaw, "Hyperspectral image processing for automatic target detection applications," *Lincoln Laboratory Journal*, vol. 14, no. 1, pp. 79–116, 2003.

[3] D. G. Manolakis, R. B. Lockwood, and T. W. Cooley, *Hyperspectral Imaging Remote Sensing: Physics, Sensors, and Algorithms*. Cambridge University Press, 2016.

[4] G. Shaw and D. Manolakis, "Signal processing for hyperspectral image exploitation," *IEEE Signal Processing Magazine*, vol. 19, no. 1, pp. 12–16, Jan 2002.

[5] L. Zhang, Q. Zhang, B. Du, X. Huang, Y. Y. Tang, and D. Tao, "Simultaneous spectral-spatial feature selection and extraction for hyperspectral images," *IEEE Transactions on Cybernetics*, vol. 48, no. 1, pp. 16–28, Jan 2018.

[6] L. Zhang, Q. Zhang, L. Zhang, D. Tao, X. Huang, and B. Du, "Ensemble manifold regularized sparse low-rank approximation for multiview feature embedding," *Pattern Recognition*, vol. 48, no. 10, pp. 3102 – 3112, 2015, discriminative Feature Learning from Big Data for Visual Recognition. [Online]. Available: http://www.sciencedirect.com/science/article/pii/S0031320314005275

[7] J. M. Bioucas-Dias, A. Plaza, G. Camps-Valls, P. Scheunders, N. Nasrabadi, and J. Chanussot, "Hyperspectral remote sensing data analysis and future challenges," *IEEE Geoscience and Remote Sensing Magazine*, vol. 1, no. 2, pp. 6–36, June 2013.

[8] A. Plaza, J. A. Benediktsson, J. W. Boardman, J. Brazile, L. Bruzzone, G. Camps-Valls, J. Chanussot, M. Fauvel, P. Gamba, A. Gualtieri, M. Marconcini, J. C. Tilton, and G. Trianni, "Recent advances in techniques for hyperspectral image processing," *Remote Sensing of Environment*, vol. 113, pp. S110 – S122, 2009, imaging Spectroscopy Special Issue. [Online]. Available: http://www.sciencedirect.com/science/article/pii/S0034425709000807

[9] D. Manolakis, E. Truslow, M. Pieper, T. Cooley, and M. Brueggeman, "Detection algorithms in hyperspectral imaging systems: An overview of practical algorithms," *IEEE Signal Processing Magazine*, vol. 31, no. 1, pp. 24–33, Jan 2014.

[10] D. Manolakis, R. Lockwood, T. Cooley, and J. Jacobson, "Is there a best hyperspectral detection algorithm?" *Proc. SPIE 7334, Algorithms and Technologies for Multispectral, Hyperspectral, and Ultraspectral Imagery XV, 733402*, 27 April 2009. [Online]. Available: https://doi.org/10.1117/12.816917

[11] D. Manolakis and G. Shaw, "Detection algorithms for hyperspectral imaging applications," *Signal Processing Magazine, IEEE*, vol. 19, no. 1, pp. 29–43, 2002.

[12] J. Frontera-Pons, M. A. Veganzones, F. Pascal, and J.-P. Ovarlez, "Hyperspectral anomaly detectors using robust estimators," *IEEE Journal of Selected Topics in Applied Earth Observations and Remote Sensing*, vol. 9, no. 2, pp. 720–731, Feb 2016.

[13] J. Frontera-Pons, J.-P. Ovarlez, and F. Pascal, "Robust anmf detection in noncentered impulsive background," *IEEE Signal Processing Letters*, vol. 24, no. 12, pp. 1891–1895, Dec 2017.

[14] J. Frontera-Pons, M. A. Veganzones, S. Velasco-Forero, F. Pascal, J. P. Ovarlez, and J. Chanussot, "Robust anomaly detection in hyperspectral imaging," in *2014 IEEE Geoscience and Remote Sensing Symposium*, July 2014, pp. 4604–4607.

[15] R. M. Cavalli, G. A. Licciardi, and J. Chanussot, "Detection of anomalies produced by buried archaeological structures using nonlinear principal component analysis applied to airborne hyperspectral image," *IEEE Journal of Selected Topics in Applied Earth Observations and Remote Sensing*, vol. 6, no. 2, pp. 659–669, April 2013.

[16] D. W. J. Stein, S. G. Beaven, L. E. Hoff, E. M. Winter, A. P. Schaum, and A. D. Stocker, "Anomaly detection from hyperspectral imagery," *IEEE Signal Processing Magazine*, vol. 19, no. 1, pp. 58–69, Jan 2002.

[17] M. T. Eismann, A. D. Stocker, and N. M. Nasrabadi, "Automated hyperspectral cueing for civilian search and rescue," *Proceedings of the IEEE*, vol. 97, no. 6, pp. 1031–1055, June 2009.

[18] N. K. Patel, C. Patnaik, S. Dutta, A. M. Shekh, and A. J. Dave, "Study of crop growth parameters using airborne imaging spectrometer data," *International Journal of Remote Sensing*, vol. 22, no. 12, pp. 2401–2411, 2001. [Online]. Available: http://www.tandfonline.com/doi/abs/10.1080/01431160117383

[19] B. Datt, T. R. McVicar, T. G. van Niel, D. L. B. Jupp, and J. S. Pearlman, "Preprocessing EO-1 Hyperion hyperspectral data to support the application of agricultural indexes," *IEEE Transactions on Geoscience and Remote Sensing*, vol. 41, pp. 1246–1259, Jun. 2003.

[20] B. Hörig, F. Kühn, F. Oschütz, and F. Lehmann, "HyMap hyperspectral remote sensing to detect hydrocarbons," *International Journal of Remote Sensing*, vol. 22, pp. 1413–1422, May 2001.

[21] A. W. Bitar, L. Cheong, and J. Ovarlez, "Target and background separation in hyperspectral imagery for automatic target detection," in *2018 IEEE International Conference on Acoustics, Speech and Signal Processing (ICASSP)*, April 2018, pp. 1598–1602.

[22] A. W. Bitar, L.-F. Cheong, and J.-P. Ovarlez, "Sparse and low-rank matrix decomposition for automatic target detection in hyperspectral imagery," *IEEE Transactions on Geoscience and Remote Sensing*, vol. 57, no. 8, pp. 5239–5251, 2019.

[23] A. W. Bitar, J.-P. Ovarlez, L.-F. Cheong, and A. Chehab, *Automatic Target Detection for Sparse Hyperspectral Images*. Cham: Springer International Publishing, 2020, pp. 435–462.

[24] J. M. F. Pons, "Robust target detection for hyperspectral imaging," Ph.D. dissertation, CentraleSupélec, 2014. [Online]. Available: https://tel.archives-ouvertes.fr/tel-01165283/document

[25] Y. Chen, A. Wiesel, and A. O. Hero, "Robust shrinkage estimation of high-dimensional covariance matrices," in *2010 IEEE Sensor Array and Multichannel Signal Processing Workshop*, Oct 2010, pp. 189–192.

[26] F. Pascal and Y. Chitour, "Shrinkage covariance matrix estimator applied to stap detection," in *2014 IEEE Workshop on Statistical Signal Processing (SSP)*, June 2014, pp. 324–327.

[27] F. Pascal, Y. Chitour, and Y. Quek, "Generalized robust shrinkage estimator and its application to stap detection problem," *IEEE Transactions on Signal Processing*, vol. 62, no. 21, pp. 5640–5651, Nov 2014.

[28] O. Ledoit and M. Wolf, "A well-conditioned estimator for large-dimensional covariance matrices," *Journal of Multivariate Analysis*, vol. 88, no. 2, pp. 365 – 411, 2004. [Online]. Available: http://www.sciencedirect.com/science/article/pii/S0047259X03000964

[29] ——, "Honey, i shrunk the sample covariance matrix," *UPF Economics and Business Working Paper*, no. 691, 2003.

[30] A. W. Bitar, J.-P. Ovarlez, and L.-F. Cheong, "Sparsity-Based Cholesky Factorization and Its Application to Hyperspectral Anomaly Detection," in *IEEE Workshop on Computational Advances in Multi-Sensor Adaptive Processing (CAMSAP-17)*, Curaçao, Dutch Antilles, December 2017. [Online]. Available: https://arxiv.org/pdf/1711.08240.pdf

[31] J. Chen and J. Yang, "Robust subspace segmentation via low-rank representation," *IEEE Transactions on Cybernetics*, vol. 44, no. 8, pp. 1432–1445, 2014.

[32] T. Cheng and B. Wang, "Decomposition model with background dictionary learning for hyperspectral target detection," *IEEE Journal of Selected Topics in Applied Earth Observations and Remote Sensing*, vol. 14, pp. 1872–1884, 2021.

[33] A. M. Baldridge, S. J. Hook, C. I. Grove, and G. Rivera, "The ASTER Spectral Library Version 2.0," *Remote Sensing of Environment*, vol. 113, pp. 711–715, 2009.

[34] R. N. Clark, G. A. Swayze, A. J. Gallagher, T. V. V. King, and W. M. Calvin, "The U. S. Geological Survey, Digital Spectral Library: Version 1: 0.2 to 3.0 micros," U.S. Geological Survey, Open file report, 1993.

[35] T. Bouwmans, A. Sobral, S. Javed, S. K. Jung, and E.-H. Zahzah, "Decomposition into low-rank plus additive matrices for background/foreground separation: A review for a comparative evaluation with a large-scale dataset," *Computer Science Review*, vol. 23, pp. 1–71, 2017. [Online]. Available: https://www.sciencedirect.com/science/article/pii/S1574013715300459

[36] X. Han, Y. Wei, H. Zhang, Q. Xu, and W. Sun, "Tuning to real for single-spectrum hyperspectral target detection," in *2023 13th Workshop on Hyperspectral Imaging and Signal Processing: Evolution in Remote Sensing (WHISPERS)*, 2023, pp. 1–5.

[37] X. Han, W. Leng, H. Zhang, W. Wang, Q. Xu, and W. Sun, "Spectral library-based spectral super-resolution under incomplete spectral coverage conditions," *IEEE Transactions on Geoscience and Remote Sensing*, vol. 62, pp. 1–12, 2024.

[38] W. Leng, X. Han, J. Deng, H. Zhang, W. Li, and W. Sun, "Spectral super-resolution by using universal and private jointed spectral library and its applications," *IEEE Transactions on Geoscience and Remote Sensing*, vol. 62, pp. 1–11, 2024.